COBEM 2023 27TH INTERNATIONAL CONGRESS OF MECHANICAL ENGENEERING

ABCM Brazilian Society of Mechanical Sciences and Engineering
27th ABCM International Congress of Mechanical Engineering
December 04-08, 2023, Florianópolis-SC, Brazil

COB-2023-1187
Analysis of Structural Robustness for Low-Cost Quadrupedal Robots

Nicolas Ferreira Cruvinel Monteiro Souza
nicolasfcmsouza@usp.br
Leonardo Felipe dos Santos
leonardo.felipe.santos@usp.br
Vivian Suzano Medeiros
viviansuzano@usp.br
Marcelo Becker
becker@sc.usp.br
Universidade de São Paulo - Escola de Engenharia de São Carlos, Av. Trabalhador Sancarlense, 400, 13566-590, São Carlos/SP, Brazil

Abstract. *The mechanical and structural design of quadruped robots is paramount to guarantee reliable operation on tasks such as industrial inspection. This study aims to rank commercially available polymer-based materials for additive manufacturing (AM) of low-cost quadruped robots. Finite element simulations are performed to assess the structural strength of a leg of the open source quadruped robot Solo fabricated with ABS, PC-ABS, PA6, PET and HDPE. The simulations encompassed static load analysis on the leg parts and impact load evaluations on the entire leg. Using a stress score criterion, PA6 emerged as the most suitable material for handling impact tests, while HDPE exhibited the lowest mass and highest lightweight characteristics. The combined score, on which both stress and mass criteria are accounted for, corroborated PA6 as an optimal choice. Future work could explore the effects of material selection on robot control dynamics, incorporating joint torque analysis. The findings provide valuable insights to select materials along the design and fabrication of legged robots, facilitating improved structural integrity and overall performance.*
Keywords: *Legged Robots, Additive Manufacturing, Finite Element Analysis, Robotics*

1. INTRODUCTION

Legged robots offer greater mobility and versatility compared to other mobile robotic platforms, such as autonomous wheeled vehicles, especially in unstructured environments such as industrial areas, agricultural terrain or mining facilities. In these circumstances, there is a growing interest in robotic platforms capable of robustly exploring the environment and autonomously collecting data. The development of legged robots, including bipedal and quadrupedal robots with bioinspired morphology like ANYmal, MIT Cheetah 3, Ghost Robotics Vision 60, and HyQReal (Bellicoso *et al.*, 2018; Bledt *et al.*, 2018; Miller *et al.*, 2020; Semini *et al.*, 2019), has been meeting this demand. The capabilities of these robotic platforms are well demonstrated in Bouman *et al.* (2020), where an autonomous exploration test circuit was performed using the quadruped robot Spot. The test involved navigating staircases, overcoming obstacles on the ground, and exploring poorly lit rooms. In particular, the robot had no prior information about the environment, such as a map. Instead, all navigation and localization were solely reliant on the robot's onboard sensors and computer.

In an effort to improve accessibility and accelerate the development of quadruped robots, open source projects are leveraging additive manufacturing (AM) with polymeric materials. This approach enables a more affordable and easily shareable mechanical design compared to designs that require the machining of metallic parts. However, the mechanical properties of the components are influenced by the AM method, such as Fused Deposition Modeling (FDM), also known as 3D printing. As a result, the structural strength and robustness of the robot may be compromised in this context (Khan *et al.*, 2022). To prevent structural failure, it is crucial to incorporate a structural design that considers the mechanical loads experienced during worst-case scenarios for the quadruped robot. Another essential factor in achieving adequate structural strength is the selection of materials. Various polymeric materials, including ABS, PLA, Nylon, and carbon fiber reinforced Nylon, are commercially available for FDM (Walia *et al.*, 2021; Delda *et al.*, 2021). While there are numerous state-of-the-art design analyses on low-cost robot manufacturing using AM, proposing methodologies for printing parameters and assembly, customized approaches are necessary for material selection based on the specific structural-dynamic loads of the robot and its intended applications.

Another advantage supported by AM is the optimization of material usage per part, leading to reduced costs and a smaller mass footprint. Decreasing the overall mass of the robot maximizes power efficiency and enhances autonomy, which is a crucial factor for mobile robots. Taking these aspects into account, the present study proposes an evaluation of commercially available FDM materials based on their mechanical load performance in the low-cost open-source quadruped robot, Solo (Grimminger *et al.*, 2020). The evaluation process considers static and dynamic load scenarios applied to one of the robot's legs, using finite element analysis (FEA). A material selection criterion is proposed based on the maximum computed von Mises stress under load and the ultimate tensile stress for each selected material. Addition-

ally, a selection criterion based on the leg's weight is introduced. As a result, a suitability ranking of the selected materials for the quadruped robot Solo is presented, considering both structural integrity and manufacturing costs.

2. DEVELOPMENT

The studies described in this paper were conducted using the Solo quadruped robot as the basis. The Solo robot is specifically designed for research purposes and incorporates various 3D printed parts to reduce the overall weight (see Fig. 3). The robot has a total mass of 2.2 kg and assumes a standard position with dimensions of 240 mm in height, 420 mm in length and 330 mm in width (Fig. 1a). A detailed view of the 2-DoF leg in its standard position is shown in Fig. 1b. The diagram in Fig. 1c represents the leg impedance control in task space.

The analytical procedure for the material selection proposal and the structural-dynamic characterization will be described. First, we discuss the FDM materials suggested for analysis. Subsequently, the finite element simulation setup, including geometry simplifications and assumed boundary conditions, will be presented.

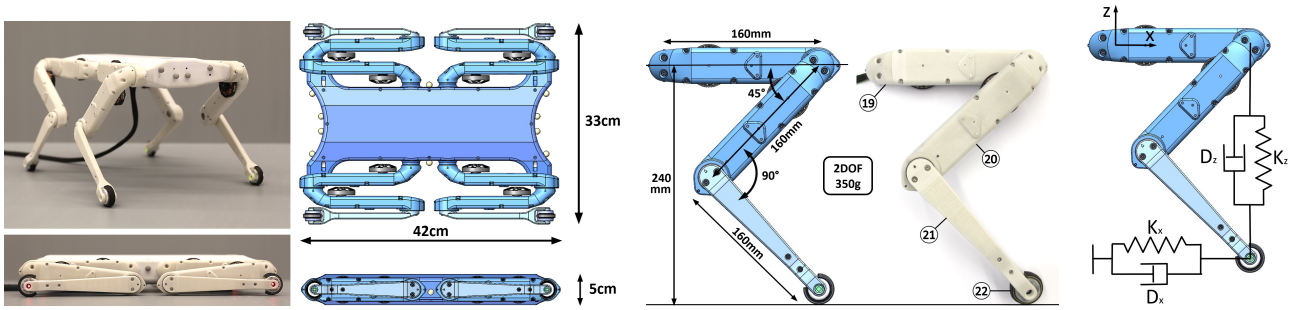

(a) Solo quadruped robot. (b) Solo's leg description. (c) Dynamic control.

Figure 1: **(a)** Solo quadruped description, showing the main dimensions and the robot assembly folded. **(b)** Solo's leg dimensions on a standard position. **(c)** Equivalent representation of the leg's dynamic control (Grimminger *et al.*, 2020).

2.1 FDM materials selection

The selection of polymer-based materials for the study took into account their printability, commercial availability, and mechanical suitability for 3D printing. The following materials were chosen: ABS, PC-ABS, PA6, PET, and HDPE. According to the official manufacturing instructions, PC-ABS is the recommended material for large structural parts, while *VisiJet M3X*, processed using stereolithography (SLA) printing, is recommended for small high-precision parts (Grimminger, 2020). Polymeric materials for 3D printing were chosen due to their lower cost compared to their metallic counterparts, which are outside the scope of the present study. Prior to conducting the finite element analysis (FEA), an assessment of the mechanical properties of the selected materials was performed. The mechanical properties presented here consider optimal settings for the geometric pattern, infill percentage, printing direction, and layer height, taking into account the wide variety of FDM printing parameters (Ali *et al.*, 2022; Kannan and Ramamoorthy, 2020; Rodríguez-Reyna *et al.*, 2022). Table 1 provides an overview of the mechanical properties of the selected materials.

Table 1: Mechanical properties of the selected materials with optimal printing parameters (Ali *et al.*, 2022; Kannan and Ramamoorthy, 2020; Rodríguez-Reyna *et al.*, 2022).

Material	**Young Modulus** MPa	**Poisson**	**Density** Kg/m^3	**Tensile Strength** MPa
ABS	2000	0.394	1020	30.0
ABS/PC	2410	0.389	1070	40.0
PA6	2620	0.340	1120	90.0
PET	2960	0.370	1420	92.9
HDPE	1070	0.410	952	22.1

2.2 Single link static load simulation

With the purpose of better understanding how the simplified 3D model of the Solo robot leg (Grimminger *et al.*, 2020) would work with the selected materials, this study makes use of a simulation phase adopting hypothesis that makes it quick to get the first results that will rank the materials. The simulation performed is a static study of stresses, in which

the materials are idealized as homogeneous and isotropics. Besides that, it is modulated around a stress-free situation where the maximum load is the robot's weight; it was assumed that the weight is equally distributed between the legs of the robot and that only two of its four legs make contact with the floor simultaneously. To further simplify the study model, only the upper part of the leg was considered, as shown in Fig. 2, disregarding the assembly in this first stage, in addition to also making use of a crimp-fixing configuration (Fig. 3a) and application of a punctual force (Fig. 3b).

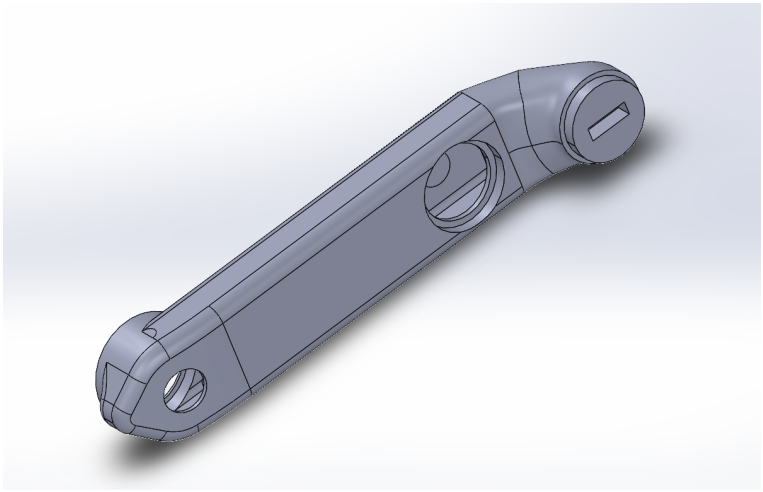

Figure 2: Part used for the first round of simulations (Model created and simulated by SolidWorks).

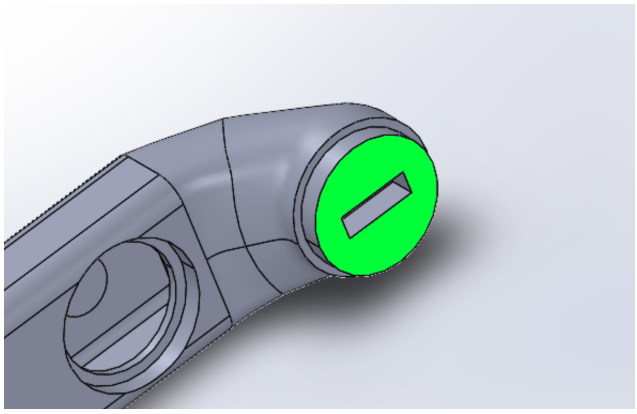

(a) Fixation.

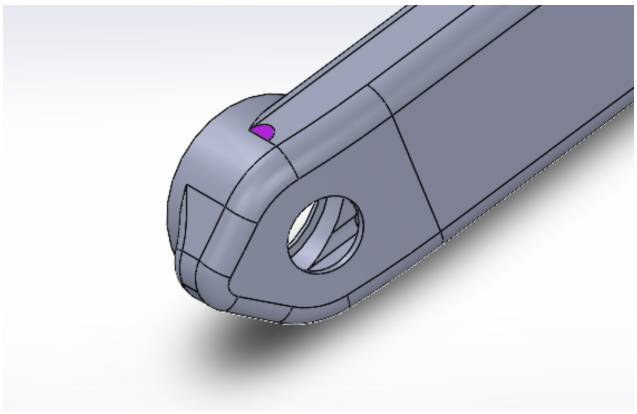

(b) Point where the force is applied.

Figure 3: **(a)** Face where the fixation was made in the simulation stress study. **(b)** Point where the point force of 10.8N was applied.

Based on our needs, the software chosen for the simulation was SolidWorks 2020, because of its ease of implementation of a static study of a piece without assembly. To complement the fixing and stressing configuration mentioned above, a high-quality mesh composed of a total of 44.527 elements was made using the SolidWorks simulation tool.

To confirm the quality of the simulation, a small survey was carried out to understand how the maximum Von Mises stress changes with the total number of elements in the mesh. For that, 5 points were plotted as shown in Fig. 4, in which it is observed that as the number of elements in the mesh increases, the maximum stress tends to stabilize. To prove this, a simple calculation can be done.

We choose the last two points of the graph and identify the maximum stress variation between them, as shown in the Eq. 1.

$$\Delta\sigma_{vM_{45}} = \sigma_{vM_5} - \sigma_{vM_4} \tag{1}$$

where $\Delta\sigma_{vM_5}$ is the maximum Von Mises stress at point 5 of the Fig. 4, $\Delta\sigma_{vM_{45}}$ at point 4 and $\Delta\sigma_{vM_{45}}$ is the difference between the two.

In percentage terms:

$$\Delta\sigma_{vM_{45}}(\%) = \frac{100}{\sigma_{vM_5}} \cdot \Delta\sigma_{vM_{45}} \tag{2}$$

With that, it can be determined that from 40,000 elements it is possible to observe the convergence of the value of the maximum Von Mises stress with a margin close to 2%.

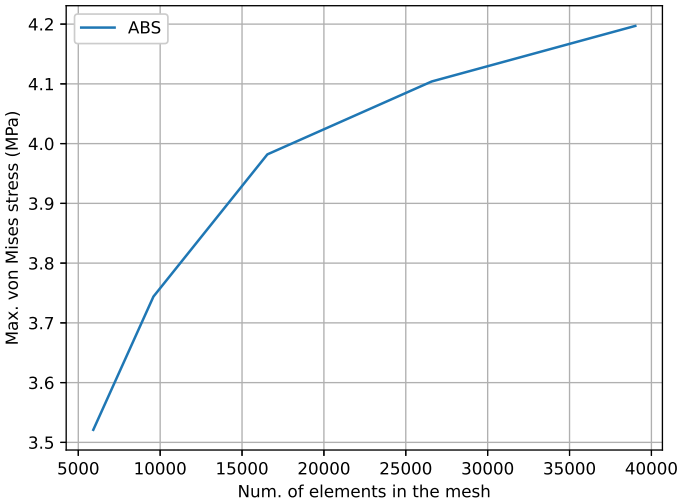

Figure 4: Maximum stress variation given a number of elements in the mesh for the ABS material.

As mentioned above, a punctual force was used in the study to simplify the model. With other simplifications already seen, the force applied in this model can be determined as:

$$F_{ol} = M_{ol} \cdot g, \tag{3}$$

where F_{ol} is the force on one leg in operation with a load of its own weight, M_{ol} represents the weight on one single leg and g is the gravity acceleration.

$$M_{ol} = \frac{M_{tot}}{2} \tag{4}$$

where M_{tot} is the robot's total mass.

Considering that in this phase, the robot is represented as if operated with its own load of 2,2 kg (Grimminger *et al.*, 2020), and that its weight is distributed between two of its four legs as shown in the Eq. 4, the force in each leg is about 1,1 kg. Using 9,81m/s^2 for gravity, a force of 10,8 N can be found from Eq. 3. This force represents the effort that a leg has to withstand given the configurations of this stage of the study, which is the value that was applied as the point force on the leg passing through all selected materials.

2.3 Three link leg impact simulation

One of the most challenging mechanical load scenarios for legged robots is jumping or recovering from a fall. A standard benchmark for evaluating the performance of a robot's leg is the vertical leg impact test (Semini *et al.*, 2010). To compare experimental and simulation results, it is valuable to simulate this specific scenario. However, to strike a balance between computational efficiency and fidelity to the mechanical model, certain constructive details were omitted during the mesh generation process. In addition, in the simulation, the materials were idealized as homogeneous and isotropic, and the behavior of the joints was approximated based on the impedance control. To simplify the leg assembly, the motors, transmission pulley, and sensors were replaced by an equivalent mass of 100 g on the hip and knee leg links.

COMSOL Multiphysics 5.1 was selected as the simulation software due to its capabilities in structural dynamics and multi-body dynamics, which are essential for accurately describing the problem at hand. The problem was set up as a transient structural 3D system using tetrahedral elements of first order. The generated mesh consists of 61.664 elements, with an average quality of 69 %. The physical configuration of the simulation replicates the experimental vertical leg impact test described in Grimminger *et al.* (2020). In the software, it was possible to constrain the degrees of freedom and create the angular joints for the leg, as well as the prismatic joint that connects the leg to a vertical slider (Fig. 5). Initially, the leg is positioned 1 mm above the surface of the base, with the collision occurring during the simulation. The

initial velocity of the leg is set to 2.1696 m/s, equivalent to falling from a height of 240 mm, matching the conditions of the experimental tests. The static friction coefficient used for the contact between the foot and the base was set to 0.8. The rotary joints were assigned stiffness and damping values that ensure that the torque acting on them is given by:

$$\tau = -k_\theta(\theta - \theta_0) - d_\theta\dot{\theta} \tag{5}$$

where k_θ is the stiffness constant, d_θ is the damping constant, θ is the corresponding joint angle, $\dot{\theta}$ is the joint velocity, and θ_0 is the joint angle equilibrium position.

For this simulation, the values used were $k_\theta = 106.06$ N.m/rad and $d_\theta = 0.3536$ N.m s/rad. These parameters characterize the behavior of the impedance control of robot joints. Although these values may not be constant over time in actual control, for the purposes of the simulation with a short time duration, constant values were adopted for k_θ and d_θ. The simulated time duration was set to 4 milliseconds, with a fixed time discretization of $\Delta t = 20$ μs. The numerical integration method employed was Generalized Alpha, $\alpha = 0.75$, representing a high-frequency dynamics damping. In this method, $\alpha = 1$ indicates no numerical damping, while $\alpha = 0$ defines maximum damping. The choice of Generalized Alpha as the integration method was made to ensure numerical stability throughout the solution (Chung and Hulbert, 1993).

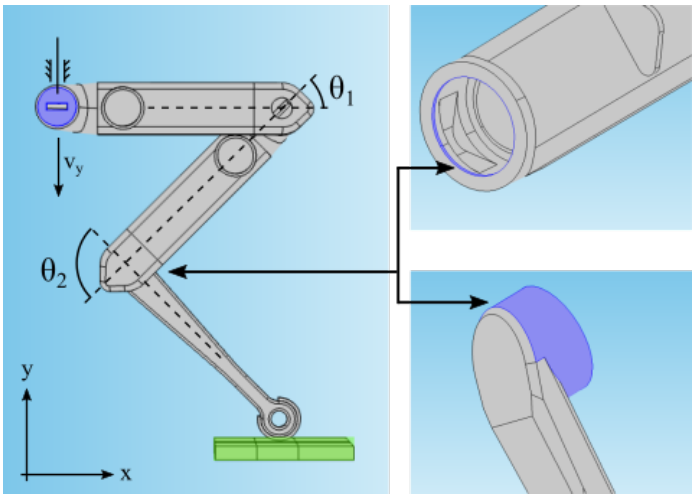

Figure 5: Physical diagram of the leg in the simulation. The blue region at the top of the leg can only move along the y-axis. The hip and knee joints are rotational. The blue surfaces seen on the right illustrate the definition of the knee joint. The base (green) is fixed, and the entire leg initially has a downward vertical velocity. The gravity vector is directed downward along the -y-axis.

The assessment of the mechanical load during the simulation is based on the von Mises stress. For each time step, the maximum von Mises stress, σ_{vM}, is computed on the entire leg and normalized by the material's tensile strength, σ_T. This process yields a stress score, S_σ, which is proposed as follows:

$$S_\sigma = \frac{1}{N_\sigma} = \frac{\sigma_T}{\max\limits_{0<t<t_d}\left[\max\limits_{\Omega}\sigma_{vM}(t)\right]} \tag{6}$$

in which N_σ is the normalized stress, t_d is the time duration, and Ω is the FEA domain representing the leg. To evaluate the leg weight according to the material, the mass score is proposed as

$$S_M = \frac{1}{gm_\Omega} \tag{7}$$

in which g is the gravity acceleration. Finally, the combined score S^* is defined as:

$$S^* = S_\sigma S_M \tag{8}$$

This score enables the ranking of materials based on the stress experienced during the impact and the weight of the assembly. The ideal material is the one that maximizes the product of the stress margin (S_σ) with the inverse of the leg weight.

3. RESULTS

This section presents the results obtained from the simulations as well as the criteria used for ranking. The simulation results provide information on the performance and behavior of the legged robot under different loading conditions. Furthermore, the proposed ranking criteria allows for the identification of materials that exhibit superior characteristics in terms of mechanical strength and weight efficiency.

3.1 Single link static load simulation

The accuracy of the results was examined with the reliability analysis shown in Fig. 4, in which we considered the mesh generated for the study satisfactory. The maximum Von Mises stress along with three ranking parameters for each material were presented in the Tab. 2.

Table 2: Impact simulation results for the maximum von Mises stress and the scores derived from it.

Material	**Max. σ_{vM} [MPa]**	**S_σ [MPa/MPa]**	**S_M [1/Kg]**	**S^* [1/Kg]**
ABS	4.365	6.873	0.809	5.560
ABS/PC	4.368	9.156	0.771	7.059
PA6	4.397	20.469	0.737	15.086
PET	4.033	22.901	0.581	13.305
HDPE	4.055	5.450	0.867	4.725

In addition to the results presented the Tab. 2, Fig. 6 shows where stress variations in the part were seen.

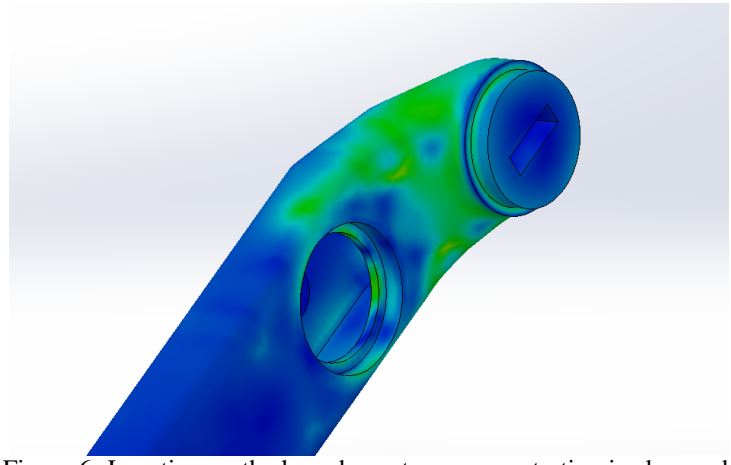

Figure 6: Location on the leg where stress concentration is observed.

From Tab. 2, we can observe that the PET material presented the lower maximum Von Mises and its tensile strength is 22.9 times higher than the maximum given in the study, providing it with an excellent margin to work safely. The PA6 is not far behind PET as its tensile strength is 20.47 times its maximum Von Mises stress, therefore, for mechanical stress, PA6 and PET are considered good options. Now, analyzing the mass score issue we see that PA6 performs better than PET which is confirmed by the analysis when balancing these two factors, where it shows that PA6 surpasses the other materials with S^* of 15,086.

3.2 Three link leg impact simulation

The accuracy of the results was assessed by examining mesh convergence before conducting the structural-dynamic analysis. The generated mesh was evaluated as satisfactory based on the von Mises stress calculations in the leg domain. The normalized maximum von Mises stress for each material, computed along the impact, is depicted in Fig. 7. Observing the graph, the impact starts at $t = 0.6$ ms, followed by a sharp decrease at $\sigma_{vM}(t)$. Subsequently, the stress exhibits an increase until the end of the simulation. Although there are significant variations over time, the maximum computed stress tends to stabilize at a lower level than that observed between 0.6 and 4.0 ms. A summary of the normalized maximum stress and the proposed scores for each material is provided in Tab. 3.

From Tab. 3, it can be observed how the proposed selection criteria are interpreted. HDPE exhibits the lowest maximum von Mises stress value; however, its tensile strength is only approximately 2.13 times higher than this value. On the other hand, PA6 shows a tensile strength that is about 4.55 times greater than the maximum von Mises stress,

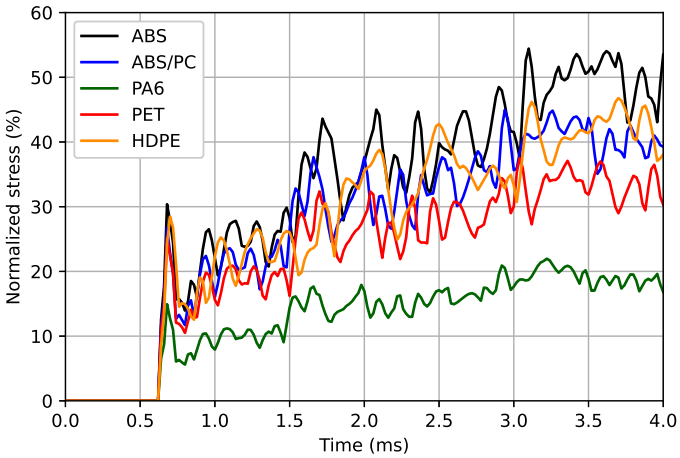

Figure 7: Normalized maximum stress during the impact simulations.

Table 3: Impact simulation results for the maximum von Mises stress and scores derived from.

Material	**Max.** σ_{vM} **[MPa]**	$\mathbf{S}_{\sigma}$ **[MPa/MPa]**	$\mathbf{S}_{\mathrm{M}}$ **[1/Kg]**	$\mathbf{S}^{*}$ **[1/Kg]**
ABS	16.33	1.837	0.809	1.486
ABS/PC	17.98	2.224	0.771	1.715
PA6	19.76	4.554	0.737	3.356
PET	21.50	2.665	0.581	1.549
HDPE	10.34	2.137	0.867	1.853

indicating a larger safety margin against mechanical stress. Consequently, when considering the stress score alone, PA6 emerges as the most suitable material. Conversely, when solely focusing on the mass score, HDPE proves to be the most suitable option due to its lower leg total mass. Finally, when balancing both factors, the combined score elevates PA6 to the highest rating, with an S^{*} value of 3.356, compared to HDPE's score of 1.853.

4. CONCLUSIONS

From a static load analysis on a leg part to an impact load assessment on the entire robot leg, the structural strength was examined, and the selected materials were ranked accordingly.

In the static load analysis on the upper part of the leg, consider a standard robot functionality, where no more than the robot's weight is used. Based on the proposed evaluation criteria, PA6 was the most suitable material in terms of resistance, while HDPE stands out as the lightest material. Considering the classification of the combination that takes into account both the lightness/density of the material, as well as its resistance, PA6 comes first, followed by PET, ABS/PC, ABS, and HDPE, in that order.

In the static load analysis on the upper part of the leg, a standard robot functionality was considered, in wich no more than the robot's own weight is used. Based on the proposed evaluation criteria, PA6 was the most suitable material in terms of resistance, while HDPE stands out as the lightest material. Considering the combined score that takes into account both the lightness/density of the material, as well as its resistance, PA6 comes first, followed by PET, ABS/PC, ABS, and HDPE, in that order.

As a potential avenue for future research, this structural assessment could be expanded to include the analysis of joint torque. This extension would not only capture mechanical stress but also evaluate the effects of material selection on the dynamics of robot control, encompassing the torque exerted on the actuators.

5. ACKNOWLEDGEMENTS

The authors would like to thank the Legged Robotics Group of the Robotics Laboratory of the São Carlos School of Engineering, University of São Paulo. This work is supported by São Paulo Research Foundation (FAPESP) under grants 2018/15472-9, and 2021/09244-6.

6. REFERENCES

Ali, L.F., Raghul, R., Ram, M.Y.M., Reddy, V.H. and Kanna, N.S., 2022. "Evaluation of the polyamide's mechanical properties for varying infill percentage in fdm process". *Materials Today: Proceedings*, Vol. 68, pp. 2509–2514.

Bellicoso, C.D., Bjelonic, M., Wellhausen, L., Holtmann, K., Günther, F., Tranzatto, M., Fankhauser, P. and Hutter, M., 2018. "Advances in real-world applications for legged robots". *Journal of Field Robotics*, Vol. 35, No. 8, pp. 1311–1326.

Bledt, G., Powell, M.J., Katz, B., Di Carlo, J., Wensing, P.M. and Kim, S., 2018. "Mit cheetah 3: Design and control of a robust, dynamic quadruped robot". In *2018 IEEE/RSJ International Conference on Intelligent Robots and Systems (IROS)*. IEEE, pp. 2245–2252.

Bouman, A., Ginting, M.F., Alatur, N., Palieri, M., Fan, D.D., Touma, T., Pailevanian, T., Kim, S.K., Otsu, K., Burdick, J. *et al.*, 2020. "Autonomous spot: Long-range autonomous exploration of extreme environments with legged locomotion". In *2020 IEEE/RSJ International Conference on Intelligent Robots and Systems (IROS)*. IEEE, pp. 2518–2525.

Chung, J. and Hulbert, G., 1993. "A time integration algorithm for structural dynamics with improved numerical dissipation: the generalized-α method".

Delda, R.N.M., Basuel, R.B., Hacla, R.P., Martinez, D.W.C., Cabibihan, J.J. and Dizon, J.R.C., 2021. "3d printing polymeric materials for robots with embedded systems". *Technologies*, Vol. 9, No. 4, p. 82.

Grimminger, F., 2020. "Details 3d printed parts". Open Robot Actuator Hardware, github.com/open-dynamic-robot-initiative/open_robot_actuator_hardware/blob/master/mechanics/actuator_module_v1/details/details_3d_printed_parts.md. Accessed 07 July 2023.

Grimminger, F., Meduri, A., Khadiv, M., Viereck, J., Wüthrich, M., Naveau, M., Berenz, V., Heim, S., Widmaier, F., Flayols, T. *et al.*, 2020. "An open torque-controlled modular robot architecture for legged locomotion research". *IEEE Robotics and Automation Letters*, Vol. 5, No. 2, pp. 3650–3657.

Kannan, S. and Ramamoorthy, M., 2020. "Mechanical characterization and experimental modal analysis of 3d printed abs, pc and pc-abs materials". *Materials Research Express*, Vol. 7, No. 1, p. 015341.

Khan, S., Joshi, K. and Deshmukh, S., 2022. "A comprehensive review on effect of printing parameters on mechanical properties of fdm printed parts". *Materials Today: Proceedings*, Vol. 50, pp. 2119–2127.

Miller, I.D., Cladera, F., Cowley, A., Shivakumar, S.S., Lee, E.S., Jarin-Lipschitz, L., Bhat, A., Rodrigues, N., Zhou, A., Cohen, A. *et al.*, 2020. "Mine tunnel exploration using multiple quadrupedal robots". *IEEE Robotics and Automation Letters*, Vol. 5, No. 2, pp. 2840–2847.

Rodríguez-Reyna, S., Mata, C., Díaz-Aguilera, J., Acevedo-Parra, H. and Tapia, F., 2022. "Mechanical properties optimization for pla, abs and nylon+ cf manufactured by 3d fdm printing". *Materials Today Communications*, Vol. 33, p. 104774.

Semini, C., Barasuol, V., Focchi, M., Boelens, C., Emara, M., Casella, S., Villarreal, O., Orsolino, R., Fink, G., Fahmi, S. *et al.*, 2019. "Brief introduction to the quadruped robot hyqreal". *Istituto di Robotica e Macchine Intelligenti (I-RIM)*.

Semini, C., Tsagarakis, N.G., Guglielmino, E. and Caldwell, D.G., 2010. "Design and experimental evaluation of the hydraulically actuated prototype leg of the hyq robot". In *2010 IEEE/RSJ International Conference on Intelligent Robots and Systems*. IEEE, pp. 3640–3645.

Walia, K., Khan, A. and Breedon, P., 2021. "Polymer-based additive manufacturing: process optimisation for low-cost industrial robotics manufacture". *Polymers*, Vol. 13, No. 16, p. 2809.

7. RESPONSIBILITY NOTICE

The authors are solely responsible for the printed material included in this paper.